

A Quantile-Based Approach to Modelling Recovery Time in Structural Health Monitoring

Alastair Gregory^{1,2}, F. Din-Houn Lau^{1,2}, and Liam Butler^{1,3}

¹Lloyd's Register Foundation's Programme for Data-Centric Engineering, Alan Turing Institute

² Department of Mathematics, Imperial College London

³Cambridge Centre for Smart Infrastructure and Construction, Department of Engineering, University of Cambridge

March 23, 2018

Keywords: Structural health monitoring, FBG sensors, streaming data, quantile estimation, stochastic recovery time

Abstract

Statistical techniques play a large role in the structural health monitoring of instrumented infrastructure, such as a railway bridge constructed with an integrated network of fibre optic sensors. One possible way to reason about the structural health of such a railway bridge, is to model the time it takes to recover to a no-load (baseline) state after a train passes over. Inherently, this recovery time is random and should be modelled statistically. This paper uses a non-parametric model, based on empirical quantile approximations, to construct a space-memory efficient baseline distribution for the streaming data from these sensors. A fast statistical test is implemented to detect deviations away from, and recovery back to, this distribution when trains pass over the bridge, yielding a recovery time. Our method assumes that there are no temporal variations in the data. A median-based detrending scheme is used to remove the temporal variations likely due to temperature changes. This allows for the continuous recording of sensor data with a space-memory constraint.

1 Introduction

Structural health monitoring (SHM) is used to maintain and monitor the structural integrity of infrastructure and assets [5], and has traditionally been implemented via expensive and time-consuming manual inspection. Recently, infrastructures have been instrumented with sensors [18, 4, 20] in an effort to understand more about the structural health of structures. Typically, the data used in SHM are the vibration responses of the structure. In this work, we use strain data to reason about structural health. It is the hope that data accrued through sensor networks will improve the maintenance and inspection of structures. With the sudden surge in available data sets from these sensors, the development of statistical methods to complement them must be pursued as a priority [9].

A key objective of SHM is to monitor a structure to detect any deterioration in it or an imminent failure. One way to detect long-term deterioration in a structure such as a bridge, is to monitor the time it takes for a structures' dynamic strain response to a specific loading event (e.g. a passing train) to return to some baseline condition (i.e. unloaded state). This duration of time will be referred to herein as the recovery time. It stands to reason that if the structure's recovery time to a specific loading event increases over time, a certain amount of deterioration or damage will have occurred. Where a network of sensors is installed to measure strain at multiple points in a structure, the recovery time at these multiple points can be monitored individually and used to isolate and determine whether deterioration is more prevalent in

certain parts of the structure. Therefore, an abundance of data from sensors fitted on to these structures provides the opportunity to use well-principled statistical techniques to model such parameters [15]. The objective of this paper is to improve the understanding of this particular aspect of SHM, via a case-study of railway bridges fitted with a network of discrete fibre optic sensors (FOS). The Cambridge Centre for Smart Infrastructure and Construction (CSIC) currently installs FOS networks on railway bridges. This work develops methodology with a view to improve the monitoring of railway bridges supported by data from these sensors, and other instrumented infrastructure in general.

The objective of modelling recovery times of structures from an event, such as a train passing over a bridge, using data accrued through a sensor network is a statistical problem. For instance, the recovery times of a bridge are random, and dependent on various factors i.e. train length, train speed, environmental factors etc. Statistical methods can be used to model such recovery times and quantify their uncertainty. This paper builds on some of the statistical techniques presented in [14] for the SHM of railway bridges. Further, we model the recovery time by understanding the baseline distribution of the FOS strain measurements. Using this baseline distribution, any changes in global behaviour of the bridge can be assessed over time.

The data that are used in this statistical study are considered in a streaming setting [14], which must be analysed in an online manner. It is assumed infeasible to store the entire data stream. Therefore, any analysis of the data in question needs to be space-memory efficient. In addition to this, the strain data collected from the FOS sensor network arrive at a high frequency (upwards of 250Hz). Many commonplace statistical methodologies have been adapted to fit into this streaming context [11, 21, 13] to include not only statistical model updates, but inference as well. For example change detection is an interesting problem in a streaming setting - the goal being the automatic detection and a switch of regime given a shift in the underlying distribution of streamed data.

To address this, statistical hypothesis tests for changes in distribution have been investigated for this streaming setting; [13] proposes algorithms for the one and two sample Kolmogorov-Smirnov tests using data that has been streamed. This and other data streaming literature considers quantile estimation [8, 1]. The objective of this estimation is to produce approximate quantiles of the streaming data, whilst only storing a fixed amount of data in space-memory. This is required for cases where sensors are continuously recording. Currently, the FOS-based monitoring system used in this study is only capable of collecting data during short intervals of time (i.e. 1–4 hours). However, the techniques developed in this paper allow continuous recording from the sensor network whilst detecting train passage events and estimating the recovery times of them. This is achieved by implementing a space-memory efficient quantile model.

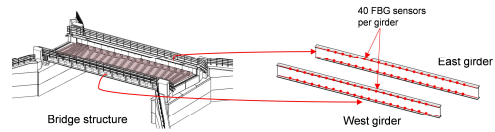
In addition to this, the underlying distribution of the sensor data considered is difficult to characterise. It is our objective to characterise this baseline distribution, under no loading, in order to determine deviations from it and also recoveries to it after a period of loading. This distribution is not Gaussian, and appears to be bounded. Fitting a Gaussian to this bounded data, would result in the likelihood of tail events being over-estimated. Due to the FOS hardware used to collect and pre-process the data, the data is also banded with a discreteness to the measured values; there are only a very small number of unique measurements. Our proposed characterisation of the baseline distribution fits alongside these properties. The non-parametric approach proposed, improves upon the work presented in [14] that assumes Gaussianity through the use of a linear model.

The data displays temporal variation that is likely due to the sensors sensitivity to temperature [12]. However it is shown in this paper that the structure of the baseline sensor data distribution remains approximately the same over time, but has a shifted median due to this temporal variation. In Sec. 6.1 a detrending approach based on a moving-median of the data is utilised to establish a baseline distribution. It will be shown that in sensor data streams that exhibit this temporal variation, the number of unique values increases with the use of detrending. Therefore a quantile-based method of characterising the data is more appropriate in this regime than other such streaming data aggregation methods (e.g. frequency counts [2, 17]).

The contribution of this paper is two-fold. First, we introduce a space-memory efficient and non-parametric quantile model for the data from a sensor network instrumented on bridges. This model uses the Greenwald-Khanna algorithm [8]. Second, we propose an algorithm that updates the quantile model whilst simultaneously checking for deviations from the baseline distribution during non-event periods.



(a)



(b)

Figure 1: An operational railway bridge instrumented with a FOS network (a), and the FOS network topology on the main bridge girders (b).

During an event, the algorithm sequentially checks for a recovery to the baseline distribution. This detection is based on a consensus of p -values from each sensor stream, every time a new data point is available. This allows the recovery time of the bridge to be estimated.

The following sections of this paper are now outlined. In the next section, specifics about the FOS data are presented. This is followed by a review of a streaming quantile estimation model used to infer information about this data in Sec. 3. A statistical test for quantile outliers, and a corresponding algorithm to detect recovery times from train passing events are presented in Sec. 4.1 and 4.2 respectively. Results from implementing the algorithm on two test cases are presented in Sec. 5, whilst results from implementing the algorithm on experimental data are given in Sec. 6.

2 Case study bridge and sensor data

Completed in April 2016, a 26.8 metre half-through steel railway bridge with a concrete composite deck carrying two lines of railway was instrumented with an advanced FOS network during its construction (refer to [14] for details). This bridge is shown in Figure 1a. The sensors are fitted on to the two girders of the bridge. As such, the strain response along the length of both girders is measured using 20 discrete FOS (spaced at one metre) installed along both the tops and bottom flanges of the girders. Figure 1b depicts the instrumented railway bridge and the FOS network topology. Together these 80 FOS make up a network which we aim to utilise in order to infer information about the structural health of the bridge they are fitted onto. The FOS used as part of this study are based on fibre Bragg gratings (FBGs). Fibre Bragg gratings are periodic variations within the core of a fibre optic cable. Each Bragg grating is created using a specific phase mask which allows the grating to reflect light at a predefined wavelength (i.e. the Bragg wavelength) with all other wavelengths of light passing through. As the fibre optic cable is strained, the Bragg wavelength shifts linearly, allowing the FBG to act as a highly stable and accurate strain sensor. Multiple individual FBGs may be inscribed along a single fibre optic cable (up to 20 FBGs) giving rise to a FBG sensor array. FOS are inherently passive and are non-corrosive and are therefore ideal sensors to be used in permanent long-term structural monitoring systems. Additional details on the operating principles of FBGs are provided in [12].

The data is measured in wavelength which is typically converted to strain. This is a useful engineering unit which can subsequently be converted into stress. Denote the wavelength from sensor $s = 1, \dots, S$ at a time t by $\lambda_t^{(s)}$. Strain measurement is computed by

$$y_t^{(s)} = \frac{(\lambda_t^{(s)} - \lambda_1^{(s)})}{0.78\lambda_1^{(s)}},$$

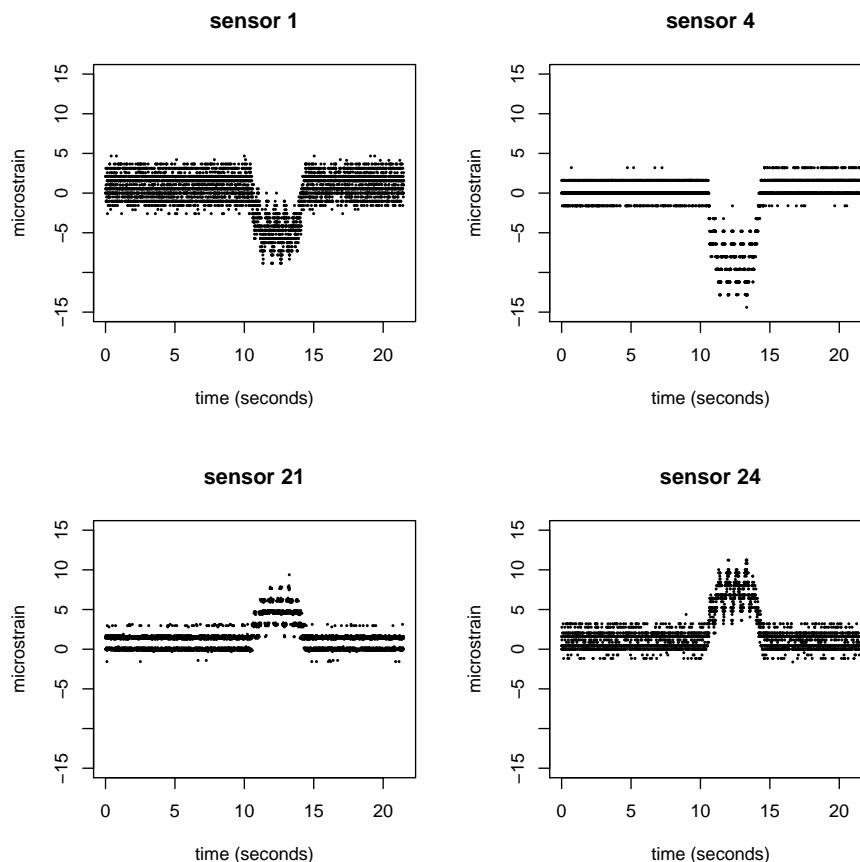


Figure 2: The microstrain measurements from four different FBG sensors at the same time during a train passage event.

where $\lambda_1^{(s)}$ is the first observed value in the stream of sensor data. Therefore it is important to note that each stream of sensor strain data is relative to the first wavelength measurement observed. Also each strain value has an approximate accuracy of ± 4 microstrain. Throughout this paper we will be working with strain measurements rather than wavelength. The acquisition rate of the data is 250Hz.

Figure 2 presents microstrain measurements from four sensors, during the same period of time when a train passes over the bridge. We shall refer to these events as train passage events. These events are noticeable in the data: a period of large-magnitude strain values. The loading period is the time interval during which the train is actually in contact with the tracks over the bridge and causes these large strain values. A number of preliminary observations can be made from Figure 2, and in particular the *baseline distribution* of the sensor data. This term will be used throughout the paper to describe the distribution of the sensor strain measurements, $\pi^{(s)}(y^{(s)})$, whilst the railway bridge is under no load. The sensors are placed in different locations on the bridge. As noted above, FBG sensors are located at various locations along the main girders of the bridge. Sensors 1 and 4 are located on the top flange of the east girder, whereas as sensors 21 and 24 are located on the bottom flange of the same girder. Note that the train passage event feature in the data from top sensors is inverted for the bottom sensors. This captures the structural mechanics principle of an Euler-Bernoulli beam in sagging bending in which the top flange of the beam is in compression (negative strain) and the bottom flange is in tension (positive strain).

The FOS interrogator hardware and software that were used to collect the FBG data use a set of pre-defined and embedded data processing algorithms written by the manufacturer. As such, the baseline distribution for each sensor exhibits a strong banding feature where only a few number unique values

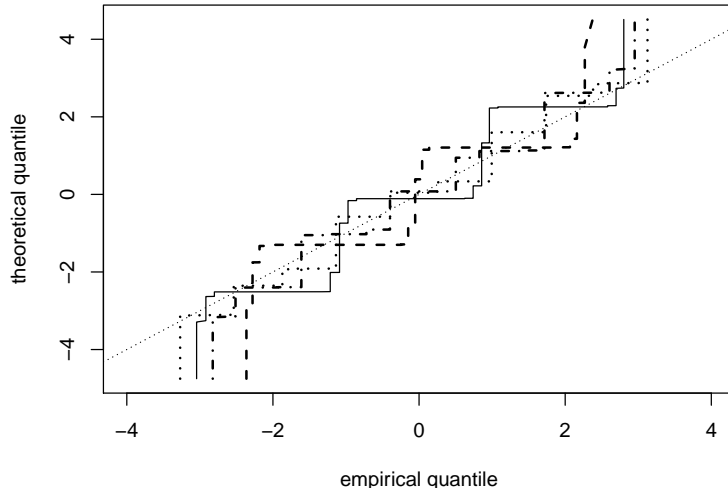


Figure 3: The empirical quantiles of four sensors with microstrain measurements (corresponding to the different line styles), over a period with no train passage events, plotted against the theoretical quantiles of a Gaussian distribution fitted to the mean and variance of each sensors strain data.

are observed. Each sensor appears to have a different number of bands. Also there appears to be a bound on the values each sensor can take which reflects the strain accuracy of the FBGs (i.e. ± 4 microstrain). Developing a framework where the baseline distributions are characterised whilst the data are being sequentially observed is an objective of this paper. The work in [10] considers the problem of characterising distributions with similar properties, and compares semi-parametric and non-parametric methods (e.g. using Gaussian mixture models).

The boundedness and banding of the sensor distributions suggest that the data is not Gaussian. The study in [14] used a Normal linear model to predict the sensor data and detect changes from the fitted model. However the banding of the data suggest that the model used is a simplification. Figure 3 shows the empirical quantiles for a set of sensor strain measurements from four different sensors against the theoretical quantiles for a Gaussian distribution fitted to the measurements. These show a disagreement with a Gaussian assumption.

Due to the fact that each strain measurement is dependent on the first wavelength measurement observed, we expect that every time the FOS analyser is reset the baseline distribution of the sensor data will shift accordingly. The baseline distribution can also shift due to temporal variations, likely due to temperature. Figure 4 shows the sensor microstrain measurements from one sensor over a longer period of time in which no train passage event occurs. Note the temporal variation in strain, however the original banding structure remains. We would like to detrend the data to obtain a baseline distribution which is invariant to these temporal shifts. We assume that the deviations away from the baseline sensor distribution of the detrended sensor data are due to train passage events only and that the baseline distribution does not change under no load.

Detrending methods, such as moving-means, can be used to remove the temporal variation from the sensor data. However, detrending using moving-means does not keep the original banding feature of the data [14]. This paper proposes to use a moving-median instead. This method also compliments and utilises the approximate quantile functions described in Sec. 3. Using the median maintains the original banding structure of the sensor strain data. The maintenance of this banding structure allows us to estimate the baseline distribution of the data excluding the temporal variations. This is described in more detail in Sec. 6.1. Note that some FOS networks may also include temperature sensors alongside strain sensors. The measured temperatures from these sensors may then be utilised to compensate for the effects of temperature on the strain sensors. However, this current study is concerned only with the temporal variations captured by the strain sensors.

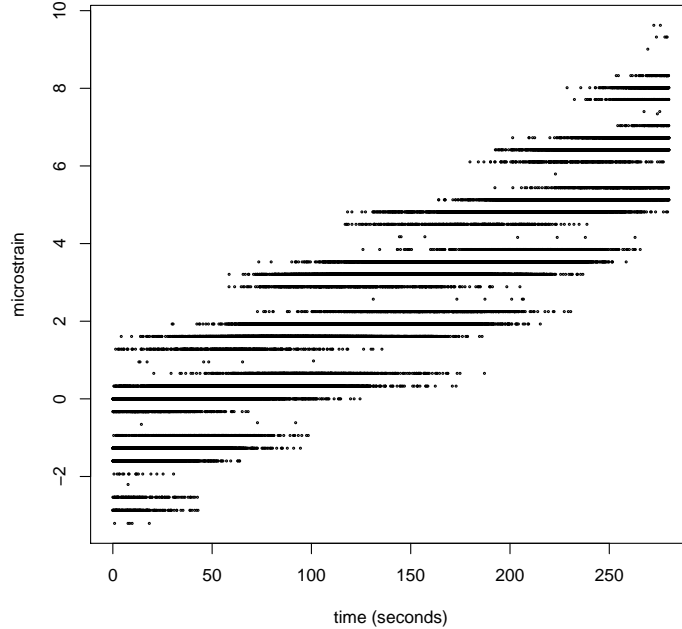


Figure 4: The microstrain measurements from a FBG sensor over a long period of time. Note the temporal shift in the baseline distribution of these measurements, likely due to temperature changes. However the banding structure of the distribution remains throughout the time period.

3 Estimating the baseline distribution of sensor data using quantiles

We model the non-parametric sensor data introduced in the Section 2 via a quantile function. A quantile function, $F^{-1}(u)$, $u \in [0, 1]$, associated with a distribution $\pi(y)$ and the random variable Y , returns the u -quantile of π_y . The u -quantile of a distribution $\pi_y(y)$ is the value of y at which the cumulative distribution function, $Pr(Y \leq y)$, crosses u . An empirical quantile function, given a set of data $\{y_i\}_{i=1}^n$, can approximate $F^{-1}(u)$ by

$$F_n^{-1}(u) = \tilde{y}_{\lceil n \times u \rceil},$$

where $\tilde{y}_1 \leq \tilde{y}_2 \leq \dots \leq \tilde{y}_n$ are the order statistics of $\{y_i\}_{i=1}^n$ and $\lceil \cdot \rceil$ denotes the ceiling function. In the case of absolutely continuous y , this is a consistent estimator of $F^{-1}(u)$. In the case of streaming data, where it is not feasible to store (and continuously sort) the whole sequence of data $\{y_i\}_{i=1}^n$, one can estimate these empirical quantiles. The studies [8, 1] cover this problem for example. We will use the Greenwald and Khanna (GK) algorithm [8]. This method is efficient in the sense that it accurately estimates the quantile function with significantly less than n data points. The algorithm is described briefly in the next section.

The GK algorithm returns a *quantile summary*, Q_n , containing $L \in \mathbb{Z}^+$ stored tuples of length 3. Each tuple contains one of the n values that has been seen in the data so far. The method is space-memory efficient since $L \ll n$. The input to this algorithm is a stream of data, and a single accuracy parameter ϵ . One can query the summary to return an approximation, $Q_n(u)$ to $F_n^{-1}(u)$, for a $u \in [0, 1]$. The summary guarantees

$$Q_n(u) \in [F_n^{-1}(u - \epsilon), F_n^{-1}(u + \epsilon)].$$

The next section explains how the algorithm works.

3.1 The Greenwald-Khanna algorithm

The GK algorithm works by keeping a set of tuples (v_i, g_i, Δ_i) , for $i = 1, \dots, L$. Let the quantile summary be given by $Q_n = \{(v_1, g_1, \Delta_1), \dots, (v_L, g_L, \Delta_L)\}$. The v_i 's are sorted so that $v_1 \leq v_2 \leq \dots \leq v_L$. These represent a subset of the values in the stream, that have been retained in the summary. Each retained v_i value is selected to cover a region of values in the original stream that have ranks between $r_{min}(v_i)$ and $r_{max}(v_i)$ in the original stream. The values g_i and Δ_i in each tuple contain the information needed to infer these minimum and maximum ranks. The g_i 's represent $r_{min}(v_i) - r_{min}(v_{i-1})$, and the Δ_i 's represent $r_{max}(v_i) - r_{min}(v_i)$ (the range of ranks that v_i cover the original stream). At any time, one can compute the maximum and minimum ranks for each summary element v_i , for $i = 1, \dots, L$, via

$$r_{min}(v_i) = \sum_{j=1}^i g_j$$

and

$$r_{max}(v_i) = \sum_{j=1}^i g_j + \Delta_i.$$

To find the values from the stream to retain in the summary, and to obtain the L tuples (v_i, g_i, Δ_i) , the algorithm iterates over two functions, **INSERT** and **COMBINE**, as follows:

COMBINE: When

$$(t \bmod (\lfloor 1/(2\epsilon) \rfloor)) = 0,$$

one can combine multiple adjacent tuples,

$$(v_{i-k}, g_{i-k}, \Delta_{i-k}), \dots, (v_i, g_i, \Delta_i),$$

into one if $g_{i-k} + \dots + g_i + \Delta_i \leq 2\epsilon t$. Note that the smallest value must in the summary must be maintained (therefore maintaining the smallest value in the stream), by requiring that $(i - k) > 1$ in the explanation of combine above. As v_i is kept in each iteration of combine, the largest value in the summary is also maintained, therefore maintaining the largest value in the stream.

INSERT: Insert the tuple, $(v, 1, \Delta)$, where v is the new value in the stream at time t , between the tuples (v_i, g_i, Δ_i) and $(v_{i+1}, g_{i+1}, \Delta_{i+1})$ where i satisfies $v_i \leq v < v_{i+1}$. Here, $\Delta = g_i + \Delta_i - 1$. If v is larger or smaller than every v_j , for $j = 1, \dots, L$, then insert $(v, 1, 0)$ at the end or start of the summary.

The algorithm is fast, and can run online indefinitely with fixed space-memory. For example, Figure 5 shows the number of elements in a quantile summary (with $\epsilon = 0.0075$) taken over a stream of values sampled from the standard normal distribution. It updates the quantile summary with this stream of values at a speed of $\sim 700\text{Hz}$ on a midrange HP laptop. For more details about the GK algorithm see [8]. Many studies have used this algorithm to obtain a summary of quantiles in a streaming data setting. Such an example is [13], where a streaming Kolmogorov-Smirnov hypothesis test uses a quantile summary constructed in this way. The next section uses a similar approach to [13] in constructing a statistical test using a quantile summary, so that a detection algorithm for recovery times from train passage events can be established in Sec. 4.2.

3.2 Inverse quantile summary queries

It is proposed in [13] that the quantile summaries described earlier in this section can approximate the empirical distribution function for a data stream. In other words, one can inversely query a quantile summary Q_n . This is achieved by a binary search of the summary values v_i , choosing the index j for which y satisfies

$$j = \begin{cases} \min(i; y \geq v_i), & y \geq v_1 \\ 0, & y < v_1, \end{cases} \quad (1)$$

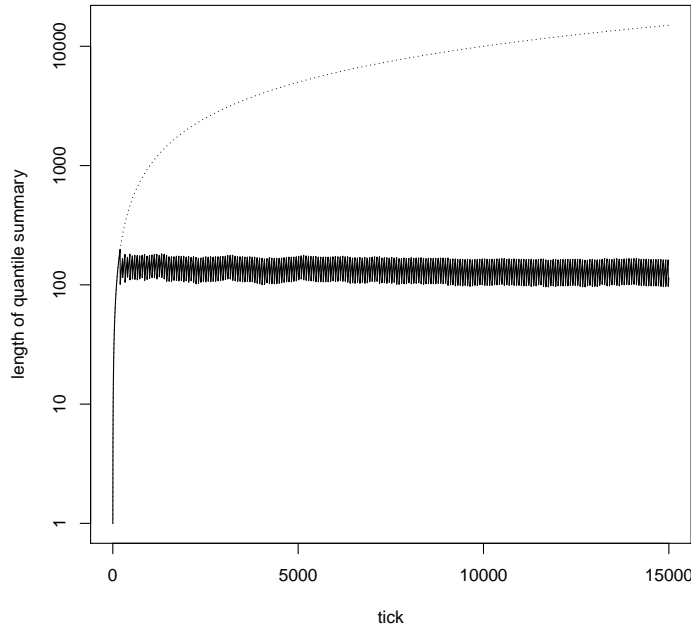


Figure 5: Number of elements in a quantile summary (solid) with $\epsilon = 0.0075$, taken over a stream of values sampled from the standard normal distribution. As the number of elements in the stream (dotted) increases, the quantile summary length remains approximately constant.

where $v_0 = -\infty$. Then one takes

$$\begin{cases} Q_n^{-1}(y) = r_{max}(v_j), & j > 0 \\ Q_n^{-1}(y) = 0, & j = 0. \end{cases} \quad (2)$$

This returns an approximation to the empirical distribution function $F_n(y) = \sum_{i=1}^n \mathbf{1}_{(y \geq y_i)}$ with an accuracy of $\pm 3\epsilon$ [13] where $\mathbf{1}$ is the indicator function.

The form of the statistical test used in the next section relies on being able to estimate p -values, by evaluating the empirical distribution function of the stream (or more specifically the summary approximation of it). Therefore we wish to have smoothed tails for our empirical estimates, as having zero p -values for any $y \geq \tilde{y}_n$ or $y < \tilde{y}_1$ overestimates the probability of accepting an experimental hypothesis in the test (by always accepting it). Smoothing in the tails is implemented by

$$\tilde{Q}_n^{-1}(y) = \begin{cases} \frac{2}{n} \phi_h(y - v_1), & y < v_1 \\ Q_n^{-1}(y), & y \in [v_1, v_L] \\ 1 - \frac{2}{n} \phi_h(v_L - y), & y > v_L. \end{cases} \quad (3)$$

where $\phi_h(y)$ is the distribution function of $N(0, h)$. As $h \rightarrow 0$, we have $\tilde{Q}_n^{-1}(y) \rightarrow Q_n^{-1}(y)$ in probability for all $y \in \mathbb{R}$. These kernels are used in well known smoothing distribution function estimates within [3], however here we only incorporate them at the tails of the empirical distribution. An important property of the Greenwald-Khanna algorithm is that the smallest and largest value in the stream are kept in the summary at all times. Denote these values \tilde{y}_1 and \tilde{y}_n . Therefore note that $Q_n^{-1}(y) = F_n(y)$ when $y \leq \tilde{y}_1$ or $y \geq \tilde{y}_n$. Using this, one notes that in the tails, $y \notin [\tilde{y}_1, \tilde{y}_n]$, we have an error of

$$|F_n(y) - \tilde{Q}_n^{-1}(y)| = |Q_n^{-1}(y) - \tilde{Q}_n^{-1}(y)| \leq 1/n.$$

Given that the quantile summary is not space-memory efficient if $\epsilon \leq 1/n$, then this error should not exceed $\pm 3\epsilon$ from the approximation $Q_n^{-1}(y)$, for $y \in [\tilde{y}_1, \tilde{y}_n]$.

4 Estimating recovery times from train passage events

The following two subsections explore how the recovery time of an instrumented bridge following a train passage event may be estimated, using a baseline sensor distribution constructed using the techniques introduced in the previous section.

4.1 A two-threshold statistical test for anomalies

In this subsection, we propose a two-threshold statistical test to detect deviations away from the baseline sensor distribution, given by the quantile model introduced in Sec. 3. This statistical test is based on the anomaly detection method used in [14], and tests the null hypothesis that strain data from all the sensors fitted onto the bridge are in the baseline state. To implement the test, we first compute p -values of each new sensor data point with respect to the baseline sensor distributions using a smoothed inverse query of the quantile models. As each new sensor point could be a deviation from the baseline distribution at either tail, the p -values take the form of

$$p_t^{(s)} = \min \left(1 - \tilde{Q}_{t-1}^{-1}(y_t^{(s)}), \tilde{Q}_{t-1}^{-1}(y_t^{(s)}) \right). \quad (4)$$

These evaluate the potential of each new data point of being extreme in comparison to the baseline sensor distribution. This statistic requires just one inverse query of the quantile summary for each sensor, and can therefore be carried out efficiently after each new set of sensor data points becomes available. We then combine p -values from all the sensors using Fishers method [6], to collect a consensus of whether the sensor data from the bridge as a whole has deviated from its baseline state. The χ^2 test statistic is given by

$$X^2 = -2 \sum_{s=1}^S \log(p_t^{(s)}). \quad (5)$$

Under the null hypothesis the statistic $(X^2 + c)$, where $c = 2S \log(0.5)$, follows a χ_{2S}^2 distribution. To see this, consider sampling $q_i \sim U[0, 1]$ i.i.d. for $i = 1, \dots, S$. These represent S p -values under the null hypothesis, for a continuous underlying distribution. Then $-2 \sum_{i=1}^S \log(q_i)$ follows a χ_{2S}^2 distribution. Let $p_i = \min(1 - q_i, q_i)$, as in (4), then $p_i \sim U[0, 0.5]$. Therefore the statistic,

$$\left(-2 \sum_{i=1}^S \log(p_i) \right) + c = -2 \sum_{i=1}^S \log(q_i),$$

follows a χ_{2S}^2 distribution.

We use two thresholds, k_l and k_u , where $k_l \leq k_u$. When a data stream is deemed in the baseline state and the value of X^2 exceeds k_u , a train passage event is signalled. On the other hand, when a data stream is signalling a train passage event and the X^2 value drops below k_l , a return to the baseline distribution is signalled. Formally, the threshold k_u corresponds to the confidence in the null hypothesis being rejected when the sensor data is currently in the baseline state. The threshold k_l corresponds to the confidence in the null hypothesis not being rejected when the train passage event is currently occurring. The value k_l should be much less than k_u .

The work in [13] considers using the Kolmogorov-Smirnov tests on the quantile summary to construct a similar type of statistical test for divergence from a distribution. However we would like to obtain a test for the deviation from (and recovery to) the baseline distribution after every new data point. Since the train passage events only last for a few seconds, we require a high temporal resolution in recovery time estimates. Whilst this can be done by using the methodology in [13], it would be inefficient as one needs to evaluate the approximate empirical distribution function at each of the v_i 's in the quantile summary

every time the test is implemented. A drawback of implementing the proposed test after every new data point is that false discoveries / deviations from the baseline distribution can occur more frequently. A future study could concentrate on the use of non-restarting and controllable CUSUM charts [7] to reduce this risk.

4.2 Algorithm

This subsection introduces an algorithm (Algorithm 1) that combines the quantile model of the baseline distribution of the sensor data (Sec. 3) and the statistical test for anomalies (Sec. 4.1), to estimate the recovery time from train passage events. The algorithm recursively tests the current sensor data point against the baseline sensor distribution, and then updates the quantile model of the baseline sensor distribution with this data point if no anomaly is detected.

Data: Strain data stream $y_t^{(s)}$ for $s = 1, \dots, N_S$ sensors and $t = 1, 2, \dots$

Input: Threshold values: $k_u > 0, k_l > 0$;

Minimum time to test for anomalies: τ .

Output: Estimated sets of start times T_S and end times T_E

Initialise $C = 0$;

for $t = 1, 2, \dots$ **do**

if $t > \tau$ **then**

 Compute p -value for each sensor using $y_t^{(s)}$;

 Compute the χ^2 test statistic, X^2 (see Sec. 4.1 for details) ;

end

if $X^2 > k_u$ and $C = 0$ **then**

 Set $C = 1$;

 Append t to the set T_S ;

end

if $X^2 < k_l$ and $C = 1$ **then**

 Set $C = 0$;

 Append t to the set T_E ;

end

while $C = 0$ **do**

 Update quantile summaries $Q_t^{(s)}$ using $y_t^{(s)}$, for $s = 1, \dots, S$ (see Sec. 3 for details);

end

end

Algorithm 1: Recovery times from train passage events

The recovery time of the sensor network is estimated by $T_E(k) - T_S(k)$ for each event $k = 1, 2, 3, \dots$. With the exception of the χ^2 test, the algorithm is run separately for each sensor, and therefore can be run in parallel. This is an improvement to the predictive linear model proposed in [14], which used information from all other sensors for each sensor.

5 Simulations

In this section, we implement Algorithm 1 on two test cases. Both test cases feature data, $\{y_t\}_{t=1,2,3,\dots}$, sampled from a baseline distribution $f_1(y)$, that at a certain time $t = T_1$ instantly changes to being sampled from another distribution $f_2(y)$. The return to the baseline distribution is then either gradual or instantaneous depending on the test case. These cases are designed to replicate a single train passage event across a sensor network. The distributions f_1 and f_2 are assumed to be unknown in our algorithm. The distribution f_1 will have a multimodal structure, similar to that found in the sensor baseline distribution (see Figure 2). Set the start time $T_1 = 1000$, the end time $T_2 = 2000$ and total number of datapoints

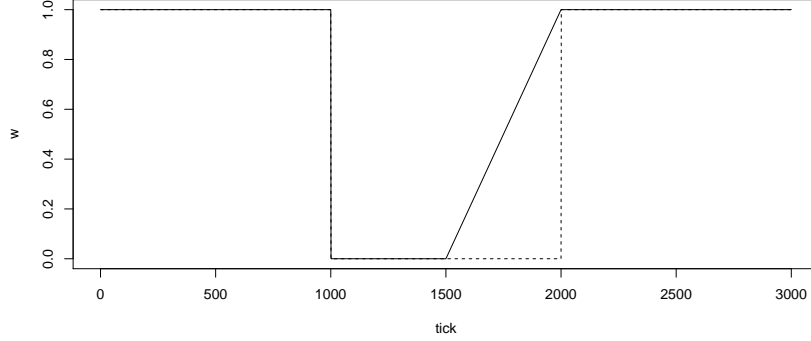


Figure 6: The values of $w^{(t)}$ for test case (1) (dashed) and test case (2) (solid).

$T_3 = 3000$. The actual recovery time of these simulations is given by the difference between end and start times, $T_2 - T_1$. Define the mixture distribution $g^{(t)}(y)$ at each time $t \in [1, T_3]$ by

$$g^{(t)}(y) = w^{(t)} f_1(y) + (1 - w^{(t)}) f_2(y),$$

where in case (1),

$$w^{(t)} = \begin{cases} 1, & t < T_1, \\ 0, & T_1 \leq t \leq T_2, \\ 1, & t > T_2, \end{cases}$$

and in case (2),

$$w^{(t)} = \begin{cases} 1, & t < T_1, \\ 0, & T_1 \leq t \leq (T_2 + T_1)/2, \\ \frac{(2t - (T_2 + T_1))}{(T_2 - T_1)}, & (T_2 + T_1)/2 < t \leq T_2, \\ 1 & t > T_2. \end{cases}$$

The values of $w^{(t)}$ for the two cases are shown in Figure 6. In these simulations, the true event start time T_1 and end time T_2 are known. Algorithm 1 outputs an estimate of the start and end times, T_S and T_E , and therefore the recovery time. We gauge the performance of our algorithm by comparing these times. The parameters utilised in Algorithm 1 are chosen to be $\epsilon = 0.0075$, $k_u = 448.5$, $k_l = 321.6$, $h = 0.2$ and $\tau = 100$. For each case, we sample $S = 100$ independent data streams, $\{y_t^{(s)}\}_{t=1}^{T_3}$, for $s = 1, \dots, S$, to simulate multiple sensors. To obtain an empirical distribution of estimated recovery times ($T_E - T_S$), 1000 iterations of the simulations are computed. The plots of $\{y_t^{(1)}\}_{t=1}^{T_3}$ and $\log(X^2)$ for a single iteration of the first and second test cases are shown in Figures 7a and 7b respectively.

For both of the test cases, the immediacy of the deviation from f_1 to f_2 at T_1 results in all 1000 iterations obtaining the exact value of $T_S = T_1$. Here $k_l \ll k_u$ to prevent false recoveries back to f_1 . To evaluate the estimated event end times, and thus the recovery times for both test cases, the empirical distribution functions of T_E are shown in Figures 8a and 8b respectively. For the first test case, none of the 1000 iterations estimate the recovery before $(T_2 + 1)$, the first point since T_1 that the data is not sampled from f_2 . For the second test case, there is a mixture of recoveries before and after T_2 amongst all of the iterations. Manually or adaptively tuning k_l , the critical value corresponding to our confidence in the data returning to the baseline distribution, could be implemented here to obtain estimates of T_E closer to T_2 .

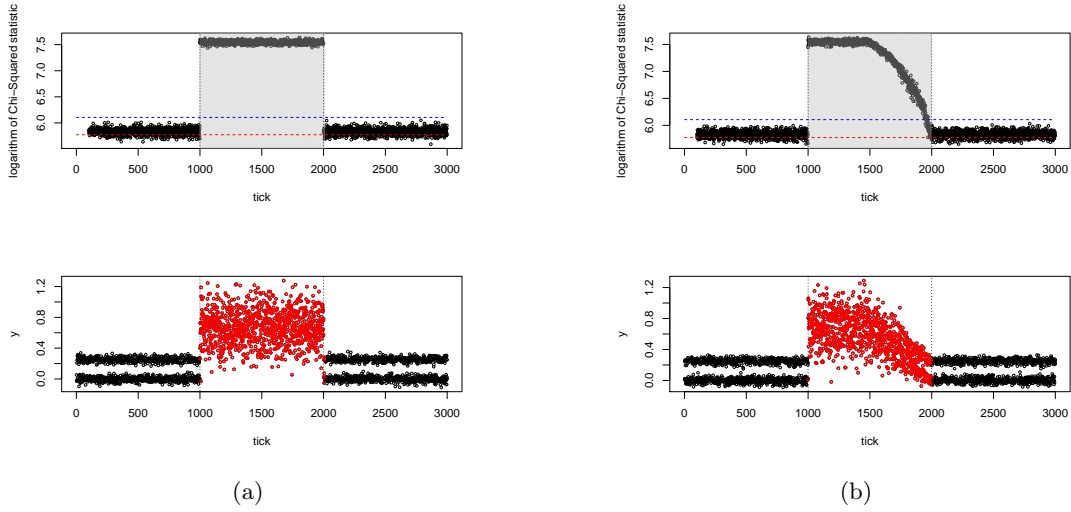


Figure 7: Plots of $\log(X^2)$ (top panels) and the data $\{y_t^{(1)}\}_{t=1}^{T_3}$ (bottom panels) for the first (a) and second (b) test cases. Black dashed lines show the prescribed start and end points, T_1 and T_2 , and the red data points / grey rectangle show the detected recovery period. In the top plots, blue and red dashed lines show the values of $\log(k_u)$ and $\log(k_l)$ respectively.

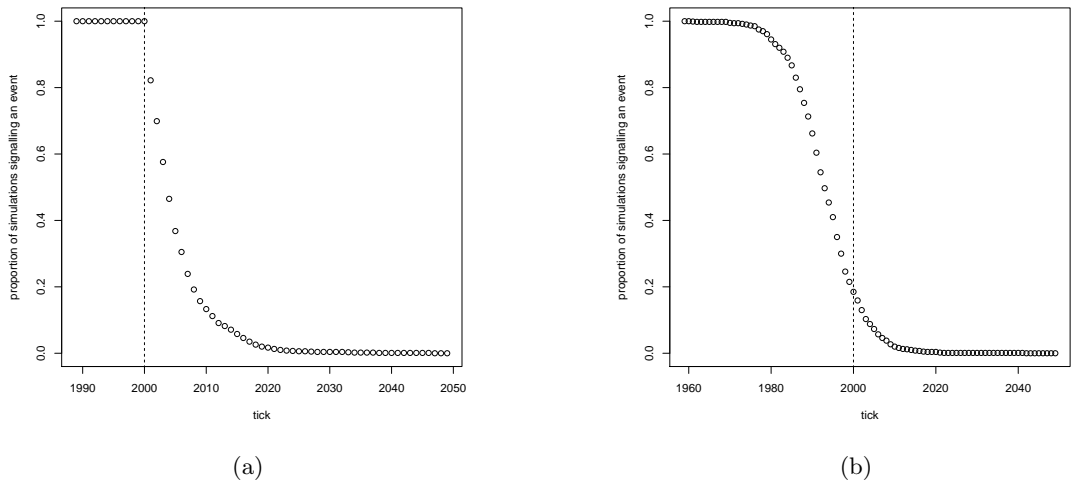


Figure 8: Empirical distribution function of T_E for all 1000 iterations of the first (a) and second (b) test cases. The black dashed line represents T_2 .

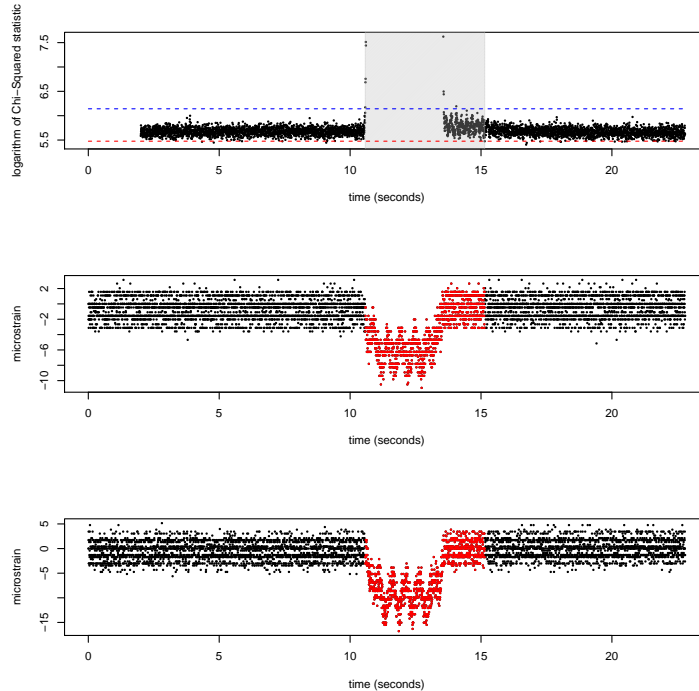


Figure 9: Plot of $\log(X^2)$ (top panel), the data from sensor 1 (middle panel) and the data from sensor 20 (bottom panel) that includes a single train passage event. The red data points / grey rectangle show the detected recovery period. In the top plot, blue and red dashed lines show the values of $\log(k_u)$ and $\log(k_l)$ respectively.

6 Application to FBG sensor data

We now use Algorithm 1 to estimate the recovery times of the bridge installed with FBG sensors. The data were recorded in July 2016 and May 2017, where 11 train passage events occurred in 2016 and 24 in 2017. Algorithm 1 is used to estimate the recovery times for all train passage events and construct baseline quantile functions for each sensor. The parameters utilised in Algorithm 1 are chosen to be $\epsilon = 0.0075$, $k_u = 464.7$, $k_l = 238.9$, $h = 0.3$ and $\tau = 500$.

Figure 9 shows the estimated recovery times for one of these events. In addition to $\log(X^2)$ over time, it shows the data streams from two sensors, 1 and 20. Sensor 1 is at the end of the girder where the train approaches from. Sensor 20 is at the other end of the girder. Therefore the start of the loading period of the train, and indeed the detected event period, occurs in the data from sensor 1 slightly before the data from sensor 20. This slight delay is noticeable in the magnified plots of the data streams in Figure 10.

The algorithm successfully picks out the train passage event using the statistical test. All 35 events were successfully detected by the algorithm. Notice that the values of X^2 take slightly longer to recover to their baseline distribution than the loading period seen in the sensor data. This indicates that the recovery time is longer than the observable loading period. During the loading period on the bridge, the p -values computed for each sensor become approximately zero, as one can see by the lack of X^2 points for this period. We note that the signal obtained from this test statistic during such an event is significantly more strong in this work, where a non-parametric quantile model is used, than that observed in [14] where a linear model is used.

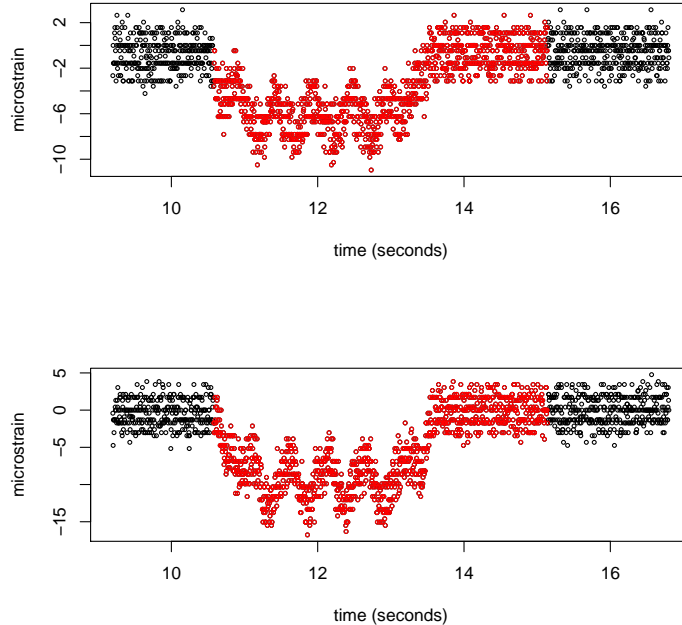


Figure 10: Magnified version of Figure 9: Data from sensor 1 (top panel) and sensor 20 (bottom panel) during a restricted time period. The red data points show the estimated recovery period.

6.1 Long and indefinite data streams

In Sec. 2, the temporal variation of the sensor strain data over long periods of time is discussed. The quantiles summaries used in Algorithm 1 assume that the data does not exhibit temporal variations. Therefore, we seek a baseline distribution of sensor data which does not exhibit temporal variation, whilst maintaining the banding structure shown in all of the sensor data. To achieve this, a moving-median detrending scheme is now proposed. Later in the subsection this scheme is used alongside Algorithm 1 to demonstrate the continuous updating of a baseline sensor strain distribution, that is free from temporal variations, and the estimation of recovery times from any train passage events.

Whilst implementing Algorithm 1 the detrended sensor data, $\hat{y}_t^{(s)}$, is now used when updating the quantile summary and computing X^2 . This modified data is given by

$$\hat{y}_t^{(s)} = \begin{cases} y_t^{(s)} + \left(Q_t^{(s)}(0.5) - \mu_{\text{med}}(y_t^{(s)}, m) \right), & C = 0 \\ y_t^{(s)} + \left(Q_t^{(s)}(0.5) - \mu_{\text{med}}(y_{T_S}^{(s)}, m) \right), & C = 1, \end{cases} \quad (6)$$

where $\mu_{\text{med}}(y_t^{(s)}, m)$ is a moving-median of the sensor data over the interval $[\max(t - m, 1), t]$. The case when $C = 1$ uses an estimate for the median of the data immediately preceding the event in question (with start time T_S). This is because the sensor data are not assumed to be from the baseline distribution during an event. The window length m is assumed small enough that the space-memory required to store the stream values used in the moving-median is negligible in comparison to that used by the quantile summary. The modifications proposed above shift the temporally varying sensor data by the difference between the moving-median and the median of the baseline distribution. An estimate for the median of the baseline distribution is stored in $Q_t^{(s)}$ (see Sec. 3), and therefore no additional computation is required. For the temporally varying sensor data shown in Figure 4, where no train passage event occurs, the values of $Q_t^{(s)}(0.5)$ and $\mu_{\text{med}}(y_t^{(s)}, m)$ are shown in Figure 11a with $m = 75$. The detrended sensor data

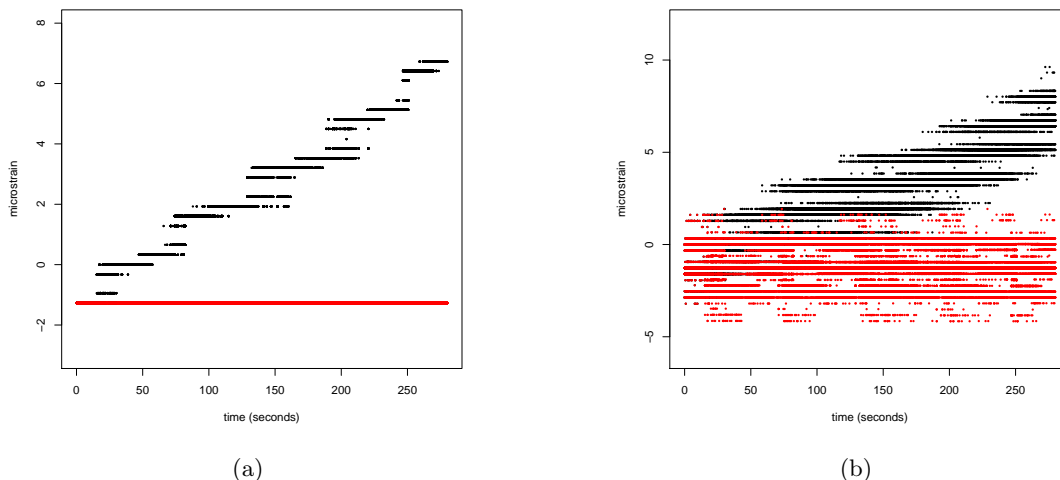


Figure 11: The values of $\mu_{\text{med}}(y_t^{(s)})$ and $Q_t^{(s)}(0.5)$ (a) and the detrended sensor data, $\hat{y}_t^{(s)}$ (b). The moving-median is shown by the black dots in (a) whilst the raw sensor data is shown by the black dots in (b). The value of $Q_t^{(s)}(0.5)$ is shown by the red dots in (a) whilst the detrended sensor data is shown by the red dots in (b).

corresponding to this data stream are shown in Figure 11b; this baseline sensor distribution maintains the banded structure of the sensor data whilst excluding any temporal variability.

The detrended baseline sensor distribution can be utilised to model recovery times from train passage events in the same way as the distribution inferred by a short, temporally invariant data set (see Figure 9). Figure 12a shows the data from a single sensor for a temporally varying data set with 222,441 points. Two train passage events occur, and the algorithm detects both of them. Here detrending has been used to infer baseline sensor distributions. The corresponding detrended data are shown in Figure 12b. Histograms with 0.25-microstrain units wide bins of both the raw and detrended data are also shown.

Figure 13 shows the size of the data stored (in megabytes) for the quantile summaries, entire data set, and frequency counts of all of the unique points in the data over time. Frequency counts can be used to construct quantile estimates in discrete data streams [17]. However the quantile summary is more space-memory efficient than using the frequency count. The temporal variability of the raw sensor data means that the number of unique values in the data increases. This suggests that the methodology presented in this paper is more appropriate in the setting of indefinite data streams.

7 Conclusion

This paper has introduced a space-memory efficient, quantile-based model for the baseline data from FBG sensors fitted to instrumented railway bridges. A baseline distribution for data from each sensor is iteratively updated in an efficient manner using an approximation to the empirical quantile function. This method also removes the temporal variation in the sensor data that are likely due to temperature changes. A novel two-threshold statistical test is used to detect a change from the baseline distribution to signal the start of a train passage event. Further, the test detects a return to the baseline distribution to signal the end of the event. Together, these event signals are used to estimate the recovery time of the sensor network, and indirectly the bridge. Future work will involve a more in-depth study of recovery times over longer time periods to reason about long-term degradation. This study may include accounting for variables such as train length, train mass, train weight and data from temperature sensors.

It is important to note that the statistical test utilised in the algorithm presented in this paper assumes that all of the sensors are independent of one another; this is not the case with the FBG sensors

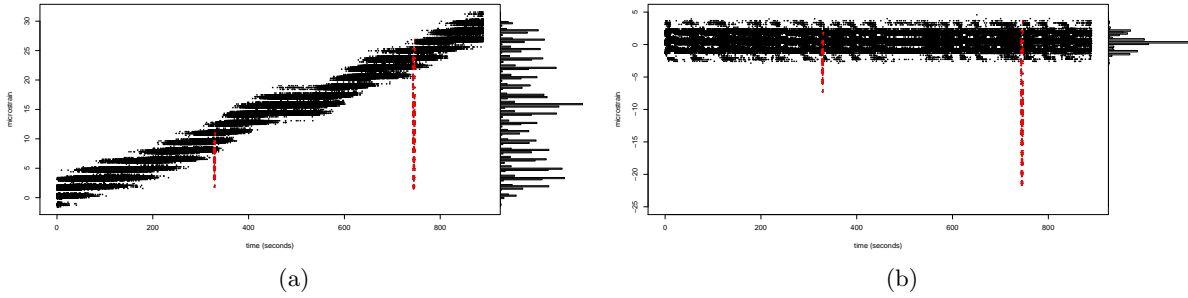


Figure 12: The raw data (a) and the detrended data (b) for a single FBG sensor over a long time interval exhibiting two train passage events. Histograms with 0.25-microstrain units wide bins for both sets of data are shown at the side of the plots. The detected train passage events are shown by the red points in both plots.

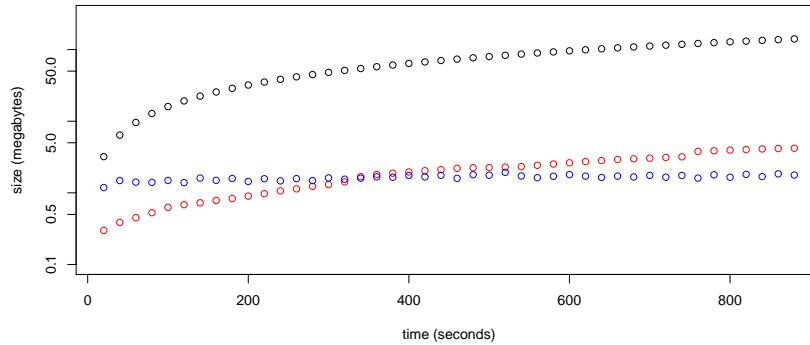


Figure 13: The combined size (in megabytes) of the detrended data sets from all sensors (black), the quantile summaries from all sensors (blue) and the frequency counts for the unique values of the detrended data sets from all sensors (red). Note that for long time series, maintaining quantile summaries for the baseline sensor distributions is space-memory efficient.

instrumenting the bridge considered here. The dependent case of the test can be implemented by Brown’s Method [16]. However, this requires a recursive covariance computation and therefore is computationally expensive for a large number of sensors. In order to alleviate this issue, a future research direction could be to reduce the dimensionality of the data before applying the methodology presented in this paper. Similarly, another important extension of this research is the spatial modelling of the sensor network, rather than treating each sensor as individual components. The dense topology of this network can be utilised by spatial statistical models of bridge recovery times and the baseline distribution of other proxies for deterioration such as curvature and neutral axis position.

The model for the baseline sensor distribution is non-parametric and features the banded and bounded structure that the data exhibits. Retaining these features is not the case when the data are modelled as, for example, a Normal linear model [14]. The work in [19] uses a similar non-parametric approach to SHM where regression models for a series of prescribed quantiles are utilised to construct a damage detection algorithm. Our methods differs from this work as we use an approximation of the empirical quantile function as the model. We combined the Greenwald-Khanna algorithm to construct space-memory efficient quantile function approximations for the baseline sensor distributions and a detrending scheme to apply the methodology to long data streams. It is our hope that this direction of research allows for the continuous recording of data from a sensor network, without the concern of memory space.

Acknowledgement

This work was supported by The Alan Turing Institute under the EPSRC grant EP/N510129/1 and the Turing-Lloyd's Register Foundation Programme for Data-Centric Engineering. The authors would also like to acknowledge EPSRC and Innovate UK (grant no. 920035) for funding this research through the Centre for Smart Infrastructure and Construction (CSIC) Innovation and Knowledge Centre. Research related to installation of the sensor system was carried out under EPSRC grant no. EP/N021614. Data related to this publication are available at the University of Cambridge data repository.

References

- [1] O. Arandjelović, D-S. Pham, and S. Venkatesh. The adaptable buffer algorithm for high quantile estimation in non-stationary data streams. In *Neural Networks (IJCNN), 2015 International Joint Conference on*, pages 1–7. IEEE, 2015.
- [2] C. Buragohain and S. Suri. Quantiles on streams. In *Encyclopedia of Database Systems*, pages 2235–2240. Springer, 2009.
- [3] M. Cheng and S. Sun. Bandwidth selection for kernel quantile estimation. In *Journal of the Chinese Statistical Association*. Citeseer, 2006.
- [4] S. Das, P. Saha, and S. K. Patro. Vibration-based damage detection techniques used for health monitoring of structures: a review. *Journal of Civil Structural Health Monitoring*, 6(3):477–507, 2016.
- [5] C. R. Farrar and K. Worden. An introduction to structural health monitoring. *Philosophical Transactions of the Royal Society of London A: Mathematical, Physical and Engineering Sciences*, 365(1851):303–315, 2007.
- [6] R.A. Fisher. *Statistical Methods For Research Workers*. Oliver and Boyd (Edinburgh), 1925.
- [7] A. Gandy and F. D-H. Lau. Non-restarting cumulative sum charts and control of the false discovery rate. *Biometrika*, 100(1):261–268, 2012.
- [8] M. Greenwald and S. Khanna. Space-efficient online computation of quantile summaries. In *ACM SIGMOD Record*, volume 30, pages 58–66. ACM, 2001.
- [9] M. R. Hernandez-Garcia and S. F. Masri. Application of statistical monitoring using latent-variable techniques for detection of faults in sensor networks. *Journal of Intelligent Material Systems and Structures*, 25(2):121–136, 2014.
- [10] Y. Hoshen, C. Arora, Y. Poleg, and S. Peleg. Efficient representation of distributions for background subtraction. In *Advanced Video and Signal Based Surveillance (AVSS), 2013 10th IEEE International Conference on*, pages 276–281. IEEE, 2013.
- [11] D. Kifer, S. Ben-David, and J. Gehrke. Detecting change in data streams. In *Proceedings of the Thirtieth international conference on Very large data bases- Volume 30*, pages 180–191. VLDB Endowment, 2004.
- [12] M. Kreuzer. Strain measurement with fiber Bragg grating sensors. 2006.
- [13] A. Lall. Data streaming algorithms for the Kolmogorov-Smirnov test. In *Big Data (Big Data), 2015 IEEE International Conference on*, pages 95–104. IEEE, 2015.
- [14] F. D-H. Lau, L. Butler, N. Adams, M. Elshafie, and M. Girolami. Some statistical methods for self-sensing bridges. In *Proceedings of the Institution of Civil Engineers - Civil Engineering*, 2018.

- [15] A. B. Noel, A. Abdaoui, T. Elfouly, M. H. Ahmed, A. Badawy, and M. S. Shehata. Structural health monitoring using wireless sensor networks: A comprehensive survey. *IEEE Communications Surveys & Tutorials*, 19(3):1403–1423, 2017.
- [16] W. Poole, D. L. Gibbs, I. Shmulevich, B. Bernard, and T. A. Knijnenburg. Combining dependent P-values with an empirical adaptation of Brown’s method. *Bioinformatics*, 32(17):i430–i436, 2016.
- [17] N. Shrivastava, C. Buragohain, D. Agrawal, and S. Suri. Medians and beyond: new aggregation techniques for sensor networks. In *Proceedings of the 2nd international conference on Embedded networked sensor systems*, pages 239–249. ACM, 2004.
- [18] M. Sun, W. J. Staszewski, and R. N. Swamy. Smart sensing technologies for structural health monitoring of civil engineering structures. *Advances in Civil Engineering*, 2010, 2010.
- [19] K. F. Tee, Y. Cai, and H-P. Chen. Structural damage detection using quantile regression. *Journal of Civil Structural Health Monitoring*, 3(1):19–31, 2013.
- [20] M. D. Todd, J. M. Nichols, S. T. Trickey, M. Seaver, C. J. Nichols, and L. N. Virgin. Bragg grating-based fibre optic sensors in structural health monitoring. *Philosophical Transactions of the Royal Society of London A: Mathematical, Physical and Engineering Sciences*, 365(1851):317–343, 2007.
- [21] M. Tveten. Multi-stream sequential change detection—using sparsity and dimension reduction. Master’s thesis, 2017.